Tuning the structure and the mechanical properties of epoxy-silica sol-gel hybrid materials

Berta Domènech,[a] Ignasi Mata*[a] and Elies Molins[a]

A new route for the synthesis of a monolithic porous hybrid organic-inorganic material composed of silica and an epoxy resin is reported. This ormosil material is prepared by supercritical drying of a gel obtained by a one-pot procedure and using ethanol as the only solvent. The microscopic analysis reveals that the material presents an open network of micrometric pores. The characteristics of the pore structure strongly depend on the ratio between silica and epoxy. While in most cases the structure is formed by homogeneous hybrid primary particles, a foam-like structure is observed for a specific composition, which seems related to a phase-separation effect. The material presents rubber-like behavior under compression. Moreover, the compression modulus can be continuously tuned along two orders of magnitude through the variation of the silica-epoxy ratio, allowing the preparation of a material with tailored mechanical properties.

Introduction

The sol-gel method is widely used for the preparation of metal-oxide porous structures from simple alkoxide precursors.[1] Noteworthy, this method is widely applied to the synthesis of aerogel, a material characterized by an open mesoporous structure, high specific surface area and very low bulk density.[2] This sol-gel process with silicon alkoxides has been studied extensively, allowing nowadays a good control on the preparation of silica pore structures. While aerogels of many oxides have been synthesized, silica aerogels are by far the most common and are moving into the market for applications mostly related to thermal insulation.[3]

While the control on the pore structure of silica aerogels allows the tuning of relevant properties of the material, the rigidity of the covalent bonds that form the silica network puts serious limitations on the mechanical properties. Thus, highly porous silica aerogels are brittle and collapse easily, being these poor mechanical properties one of the main drawbacks for their general use.

An approach proposed for overcoming this important limitation is the preparation of hybrid materials that combine silica with organic compounds that add flexibility or robustness to the pore structure. For example, the coating of the silica pore structure with organic polymers in crosslinked aerogels[4, 5] has demonstrated to add robustness to the material, reducing brittleness. Alternatively, bridged precursors have been used in the preparation of silsesquioxane aerogels where the organic chains are incorporated into the network structure,[6, 7] giving flexibility to the material. Thus, in order to obtain the best features both methods can be combined in the same material.[8, 9] In this sense, the use of crosslinked and bridged precursors can successfully enhance the mechanical properties over pure silica materials. However, this comes at the cost of a much more complex synthesis route. In the case of crosslinked aerogels, the coating is prepared after a treatment of a silica gel that requires, in some cases, replacing several times the solvent in the pores. Moreover, some precursors are not reactants of common use and can be difficult to synthesize.

Taking into account that silica gels can be easily prepared using ethanol as the only solvent, the use of ethanol soluble epoxy resins in the preparation of such hybrid materials seems to be a good idea since it avoids the use of other solvents in the preparation of the material. Epoxy resins have been used in the preparation of epoxy/silica hybrid materials[10] using a wide diversity of synthesis routes based on the sol-gel method.[11, 12] Moreover, epoxy-silica hybrid materials can be prepared by one-pot synthesis,[13] avoiding the use of large amount of solvent and the complexity of replacing the solvent filling the pores in the gel. Moreover, the use of solvents common in polymer synthesis, much less environmentally friendly than ethanol, can be completely avoided.

Up to now, epoxy resins have been used in the preparation of crosslinked aerogels following a one-pot synthesis.[13] Usually, the coating is obtained after reaction of the epoxy groups in the resin with amine groups previously attached to the surface of the silica gel. In fact, the reaction of epoxy groups with amines has been also used in the synthesis of bridged precursors for the

preparation of hybrid porous materials.[14] While the bridged precursor was originally obtained from the reaction of two silicon alkoxides, one containing the epoxy and the other the amino groups, it has been suggested that a bridged precursor could also be obtained by reacting an epoxy resin and an aminated silicon alkoxide.[15]

In this work, a new hybrid porous material has been developed from the reaction of an epoxy resin and silicon alkoxides. The gel is prepared following a new one-pot method and using ethanol as the single solvent, with the epoxy-resin included as a co-precursor with silane active groups able to generate organic bridges in-between the silica network, instead of only as a cross-linker. The measurement of the compression modulus reveals that the mechanical properties can be tuned along two orders of magnitude just by modifying the molar ratio between alkoxides and resin. These results demonstrate the possibility of preparing hybrid porous materials with tailored properties by environmentally friendly methods.

Materials and experiments

Materials

Tetraethoxysilane (TEOS), bisphenol-A propoxylate diglycidyl ether (BPGE) and (3-aminopropyl)triethoxysilane (APTES), ammonia (NH_3) and ammonium fluoride (NH_4F) were all purchased from Sigma-Aldrich. Ethanol 96% (EtOH) was purchased from Panreac. The catalytic basic solution was prepared by mixing the same volumetric amount of NH_3 30% and NH_4F 0.5 M. In all the experiments, distilled water was used. All reagents were used without further purification.

Preparation of monoliths

Gels were prepared via a one-step procedure, by combining a first pre-formed organo-modified co-precursor with the other reactants, in a sol–gel process. In a typical procedure in order to obtain the bridged precursor a certain amount of APTES is mixed with BPGE in EtOH with a molar ratio BPGE/APTES = 0.5, and the mixture is placed in the oven at 60 ºC for 1h. The reaction between the glycidyl ether groups of the epoxies with the amines of APTES is expected to occur through simple addition (Figure 1).

Afterwards TEOS is added to the cooled solution under magnetic stirring. After mixing for 5 min, water and the basic catalyst,

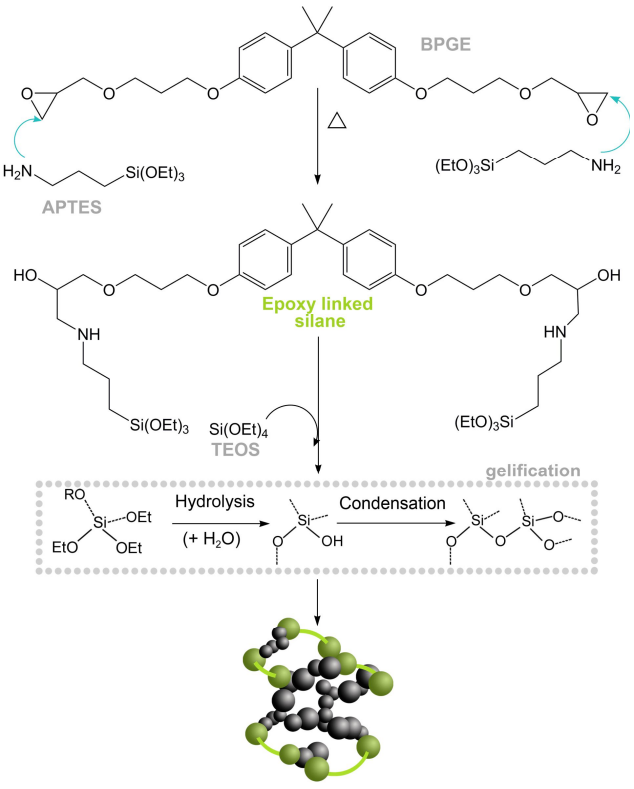

Fig. 1 Scheme reaction for the formation of the hybrid gels. For the sake of clarification, in the gelification step R may stand either for ethyl (TEOS) or the APTES-epoxy bridge (epoxy linked silane).

previously prepared by mixing the same volumetric amounts of NH_3 30 % and NH_4F 0.5 M, are added together to the mixture, which is again stirred for 3 min and placed in the corresponding molds. All gels were prepared with a molar ratio H_2O/Si = 15, EtOH/Si = 12 and NH_4OH/Si = 0.01. Si stands here for the total amount of silicon, which is the sum of TEOS and APTES.

Samples with different proportion of TEOS and APTES were prepared (Table 1) keeping the amount of silicon constant. As the ratio BPGE/APTES is fixed, the proportion of the total silicon coming from APTES (r_{APTES}) is also a measure of the amount of epoxy present in the material. The samples are identified by the code Ax, where x = 100 r_{APTES} is the percentage of silicon coming from APTES.

Table 1 Properties of the synthesized materials.

CODE	r_{APTES}	t_{gel} (min)	ρ_{bulk} (g/cm^3)	$\emptyset_{shrink}$ (%)	E (MPa)
A0	0.00	24	-	-	-
A5	0.05	-	-	-	-
A10	0.10	25	-	-	-
A11	0.11	56	-	-	-
A15	0.15	18	0.10	0.7	-
A25	0.25	14	0.14	1.4	0.60
A30	0.30	11	-	-	0.66
A35	0.35	14	0.19	6.8	0.71
A40	0.40	13	0.23	3.4	0.89
A45	0.45	15	0.21	4.5	1.45
A50	0.50	13	0.23	7.2	2.82
A55	0.55	24	0.25	6.8	2.11
A60	0.60	20	0.26	5.3	2.54
A65	0.65	22	0.23	8.5	-
A70	0.70	35	0.26	8.0	7.38
A75	0.75	63	0.26	11.0	11.69
A80	0.80	60	0.30	13.6	22.60
A85	0.85	120	0.33	9.1	-
A90	0.90	90	0.34	15.5	62.76
A95	0.95	180	0.32	8.7	-
A100	1.00	180	0.54	21.2	79.91

After gelation, which takes between 10 to 180 min depending on the composition of the solution, gels are covered with EtOH in order to allow them to age for 24 h at room temperature. After that time, gels are extracted from the molds (Ø = 0.65 cm) and placed in a vessel with fresh solvent. In order to remove any possible impurity or non-reacted species, solvent solution is replaced with fresh solvent twice in intervals of 24 h.

Note from Table 1 that a classical silica aerogel (A0) - prepared by adding water and the basic catalyst (prepared by mixing the same volumetric amounts of NH_3 30 % and NH_4F 0.5 M) to TEOS in EtOH (molar ratio H_2O/Si = 15, EtOH/Si = 12 and NH_4OH/Si = 0.01) - is included for comparison.

In order to dry the as-prepared gels supercritical drying is used. To do so, gels are placed in a 300 mL reactor and pressurized to 100 bar by introducing liquid CO_2. After removing the EtOH by circulating liquid CO_2 during 2 hours, the temperature is raised up to 40 ºC by a thermal bath, bringing CO_2 to the supercritical state. After 1.5 hours of additional CO_2 circulation, the reactor is closed during 0.5 hours, and afterwards CO_2 is brought to gas state by slowly depressurizing the reactor. Finally, the reactor is cooled to room temperature.

Characterization

The bulk density (ρ_{bulk}) of the monoliths was determined by a simple measuring with a Vernier caliper and weighing with a Sartorius CPA225D the samples.

The oxidative removal of the organic fraction was monitored via thermogravimetric analysis (TGA) and differential scanning calorimetry/differential thermal analysis (heat flow DSC /DTA) system NETZSCH -STA 449 F1 Jupiter, under air conditions and up to 800 ºC.

Surface areas were evaluated by nitrogen adsorption isotherms, which were measured with a Micrometrics ASAP-2000 (degasification at 80 ºC and vacuum 0.05 mbar). The analysis of the adsorption and desorption isotherms was done with the Brunauer-Emmett-Teller (BET) model.

For a three-dimensional visualization of the pore structure scanning electron microscopy images (SEM) were acquired with a Quanta FEI 200 FEG-ESEM, and transmission electron microscopy (TEM) images were obtained with a 120 kV JEOL 1210.

The elastic properties of the gels were determined with a DMA Q800 from TA Instruments. Compression experiments were performed with cylindrical monoliths. The monoliths were compressed at 1 N/min until 18 N, which is the maximum force allowed by the device.

Results

Structure

The different monoliths prepared and their main characteristics are given in Table 1. Gels were prepared and successfully dried for all tested compositions but A5, which is the one containing less amount of polymer. In this case, a particulate sol was obtained. The formation of a sol in A5 can be attributed to the catalytic action of a small amount of unreacted amino groups in the APTES. The action of the APTES as a basic catalyst is well known.[16] This kind of catalyst accelerates the hydrolysis of the alkoxide groups while retarding the formation of siloxane bridges of the silica,[17] favouring the formation of the particulate sol.

It can be supposed that the same catalytic action of the APTES is present along all the series in Table 1. Indeed, gels with lower amount of organic part ($0 < r_{APTES} < 0.15$) present slight white colour and blobby aspect, which are indicative of a particulate sol. For larger amount of epoxy the final material is more robust, indicating that the consistency of the gel comes from the action of the epoxy.

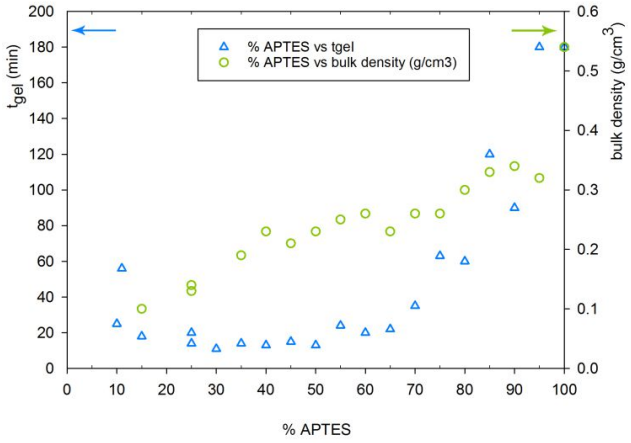

Fig. 2 Gelification time (t_{gel}) and bulk density vs the percentage of APTES. The increase in ρ_{bulk} with % APTES is related to the increasing amount of epoxy resin while the behaviour of tgel can be explained in terms of the formation of a phase rich is silica precursors.

In general, the density of the material tends to increase with the proportion of APTES (Figure 2) as expected for the increasing amount of epoxy-resin included in the sample. This amount of organic material can be clearly assessed by TGA, since the degradation of the epoxy is observed as a mass loss in the range 200 – 800 ºC, being the mass remaining at the end of the scan corresponding to the silica. Results presented in Figure 3 correspond to the total mass loss observed in each sample after the thermal treatment. As it can be observed, experimental results match almost perfectly with the theoretical amount of organic species calculated for each case. The only value which is not fully consistent with the theoretical amount, which should be zero, is the one corresponding to 0 % of APTES. In that case, the loss observed is around the 10 % instead of the 0 % that could be expected. The difference observed between these two values may be explained due to the presence of non-hydrolyzed ethoxy groups that could remain attached to the silica structure once the gel was formed. Thus, it can be assumed that almost all the epoxy is immobilized in the monoliths as it is not removed during the washings and the drying of the gel.

The amount of BPGE and APTES has also an important effect on the morphology of the pore structure, as can be observed in the

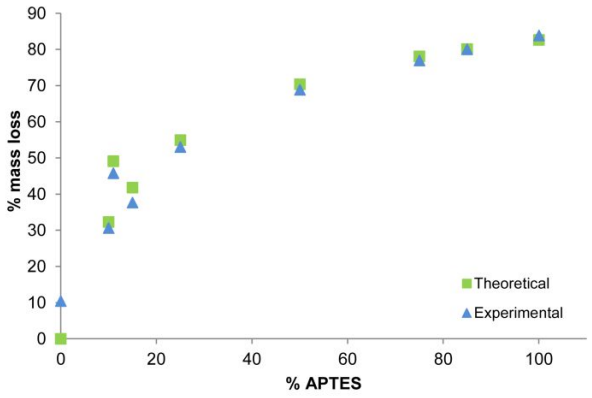

Fig. 3 Percent of mass loss of the samples as a function of the percentage of APTES. The theoretical value is calculated from the composition assuming that the mass loss comes from the degradation of the organic part of the epoxy-linked silane. According to this result, all the epoxy resin is incorporated to the final material.

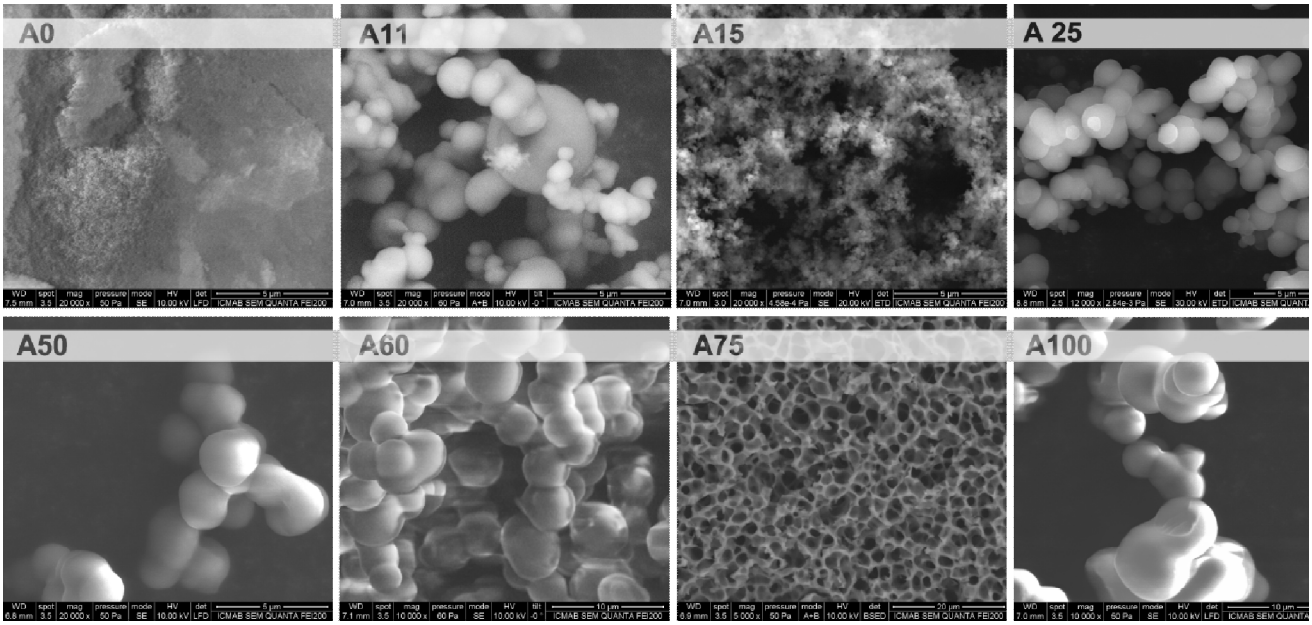

Fig. 4 SEM images of some of the samples. All images are at 20000X except A100 and A60, which are at 10000X and A75, which is at 5000X. The microstructures from A15 to A100 are explained for the solidification of a phase rich in polymer and silicon precursors, with the differences between them arising from the increasing bridged precursor/TEOS ratio. A0 and A11 are driven by the hydrolysis and condensation of TEOS without the formation of this rich phase.

SEM images (Figure 4). In most cases, the pore structure is formed by assembled particles of micrometric size. In fact, similar structures built of pure silica obtained following a completely different sol-gel procedure have also been reported.[18] Moreover, the small surface areas observed by BET analysis, lower than 15 m^2/g in all cases, confirm that there are no pores with sizes below 50 nm. Thus, it can be concluded that the only pores present are the micrometric pores observed in the images of the Figure 4. On the contrary, these microparticles are not observed in A15 and A75, being replaced by conglomerates of nanoparticles in A15 while in A75 a foam-like structure is observed.

In order to understand the effect of the amount of epoxy-resin on the morphology of the pore structure, it should be taken into account that, besides the sol-gel transition, the presence of the epoxy can induce the phase separation processes common in polymer science. The interplay of sol-gel and phase separation can induce the formation of complex pore structures,[19] which has been extensively exploited in the design of porous materials from silsesquioxane precursors.[20] Thus, a possible explanation of the images in Figure 4 could be the formation by phase separation of a phase rich in polymer and silica-precursor. The gel would form by condensation of the silanol groups in this phase. The particles in samples with $0.15 \leq r_{APTES} \leq 0.60$, with growing sizes as the amount of polymer increases, would correspond to the solidification of this precursor rich phase.

A closer look to these particles can be achieved by TEM images (Figure 5). As observed, while A15 is formed by nanoparticles up to 50 nm, A25 seems to be composed of an agglomerate of nanoparticles of similar size. These nanoparticles are similar to the silica nanoparticles that form the solid skeleton in classical silica aerogels, although they should include organic bridges in their composition, as in the case of ormosils.[21] While in aerogels these particles polymerize forming a mesoporous structure, in this case they agglomerate in the rich phase, which becomes the solid part of the final material.

The progression of growing particle size observed in the range $0.15 \leq r_{APTES} \leq 0.60$ breaks suddenly in the foam-like structure of A75 (Figure 4). For this large concentration of polymer, no nanoparticles are observed (Figure 5) appearing a continuous solid. The microstructure of A100 is similar to samples in the range $0.15 \leq r_{APTES} \leq 0.60$, although the particle size and the pores are much larger (Figure 4).

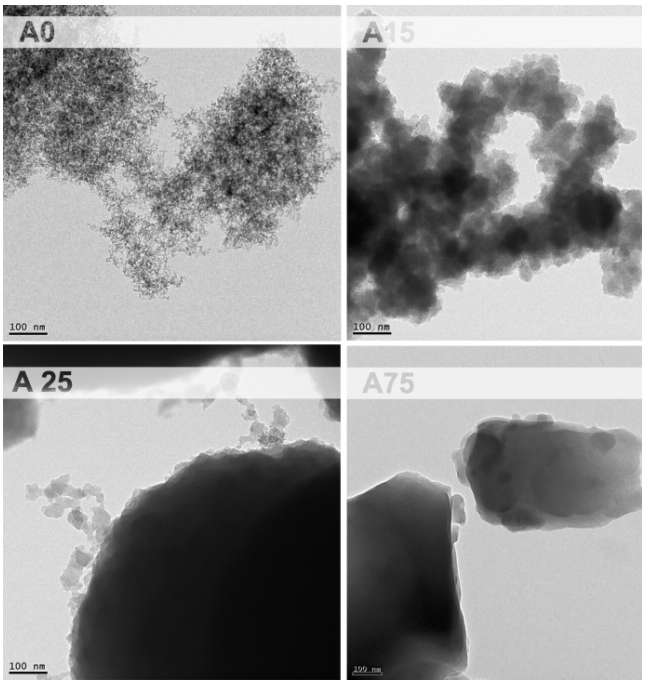

Fig. 5 TEM images of materials prepared with different amount of epoxy-resin. A0 corresponds to a common silica aerogel, A15 and A25 seem formed by the agglomeration of nanoparticles and A75 appears as a continuous solid.

These changes in the microstructure are accompanied by a significant increase in the gelification time (t_{gel}) for the samples with $r_{APTES} \geq 0.75$. A75 corresponds to the particular case with ratio bridged precursor/TEOS = 1.5. The structure of aerogels synthesized from a combination of a bridged precursor and TEOS is, in principle, formed by small silica particles connected by organic bridges [9]. However, with the large concentrations of bridged precursor present in samples with high concentration of APTES, the structure of the material should be closer to a silsesquioxane aerogel, formed by a continuous of silicon atoms connected by organic bridges.[22] The sudden change on the pore structure that takes place at r_{APTES} seems to be related to a transition between a pore structure dominated by bridged silica particles ($r_{APTES} \leq 0.60$) or by bridged SiO_4 moieties ($r_{APTES} \geq 0.75$). Moreover, the larger shrinkage ($\emptyset_{shrink}$) of the samples with $r_{APTES} \geq 0.75$ (Table 1) can be caused by solvent retained by the rich phase after the gelification and removed during the drying.

As an aside, the growing size of the particles observed can be related to the trend shown by t_{gel}. The gelification time tends to increase with the amount of APTES (see Table 1 and Figure 2), which could be related to the progressive lowering in the amount of ethoxy groups as this tri-ethoxy precursor replaces TEOS. The dynamics of phase separation drives toward a reduction in the total interface between phases, favoring the growth of large bulky domains. As more time is needed for the gelification of the rich phase, this process is more advanced and particles are larger.

Finally, the large particles observed in A11 (Figure 4) suggest that phase separation does not take place for these low amounts of polymer. It can be assumed that the pore structure results from the formation of silica particles that eventually coalesce in the gel following the common scheme of the sol-gel process. The absence of a rich phase with high concentration of silica precursors can also explain the large t_{gel} for samples with $r_{APTES} \leq 0.11$ in spite of presenting the largest concentration of ethoxy groups.

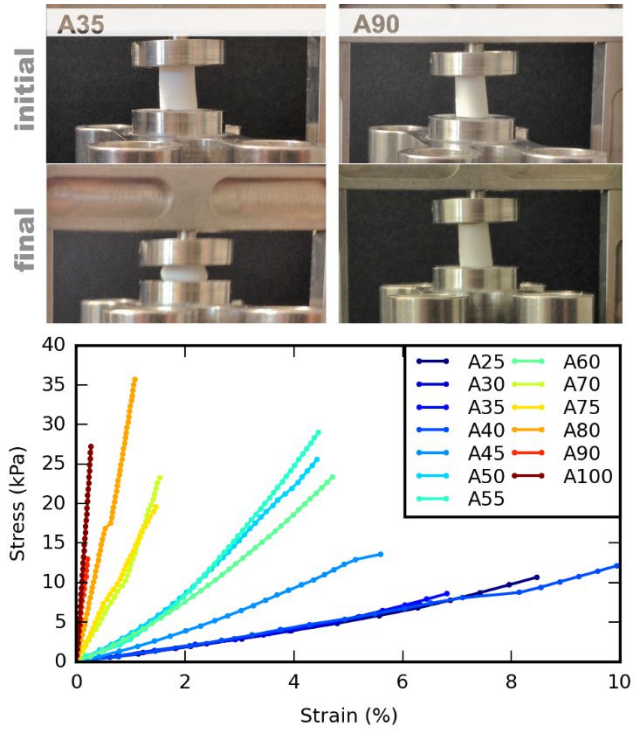

Fig. 6 Photographs of two samples at the beginning and end of the compression test (top) and the corresponding stress-strain curves (bottom). In the top, a clear variation in the length of A35 before and after compression is observed, while variations in the length of A90 were not evident at the naked eye. Small differences in the images for A90 before and after compression are caused by the different angle at which the photo was taken.

Mechanical properties

The dramatic changes in the pore structure of the material when varying r_{APTES} has important consequences in the mechanical properties of the material.

While the samples with lowest r_{APTES} crumble easily, samples with largest values of r_{APTES} are difficult to break. The compression modulus could only be measured for samples with $r_{APTES} \geq 0.35$ because of the frailty of samples with $r_{APTES} \leq 0.35$.

In general, under compression the material presents a rubber-like behavior, appearing a continuous increase in the slope of the stress-strain curve that makes difficult to define a linear domain for the calculation of the apparent modulus (E_a). The measured samples with lower r_{APTES} are very flexible (Figure 6) and do not present a clearly defined linear domain in the stress-strain curve. In fact, the strain at the maximum applied force (18 N) can be as high as the 80 %.

The compression modulus was calculated after fitting the lowest 10 % of the stress-strain curves (15 % for A35 because of the low number of points in this range) to parabolas and taking the apparent modulus E_a from the derivatives at zero strain, following a procedure previously applied to rubbers.[23] The elastic modulus (E) can be calculated from E_a, the Poisson's ratio ν and the shape factor S, which is defined as the radius divided by the height in the case of cylindrical samples.[24] A standard value of ν = 0.5, corresponding to an uncompressible material, was taken. The elastic module of the samples was calculated from Equation 1:

$$E = \frac{2}{2+S^2} E_a \qquad (1)$$

The values of E calculated (Table 1) are 0.823-0.942 E_a for the measured samples. If the material is compressible, which cannot be excluded, the elastic modulus would be slightly larger, but always lower than E_a. As an example, with ν = 1/3, which is a generic value for rubber, [25] E is 4 -14% larger than in the uncompressible case.

The module of the samples fall in the range of polymer foams and elastomers, being the density intermediate between both kind of polymeric materials.[26] Similar values of E have been also observed in silica aerogels prepared from trialkoxide precursors.[27]

In our case, E increases continuously with r_{APTES} along two orders or magnitudes, as can be observed in Figure 7. Error bars in this Figure are calculated from error propagation of Equation 1 taking the standard uncertainty of S from the experimental error in the measurement of the sample dimensions while for E_a the standard deviation of the corresponding parameter in the least squares fit was used. As can be observed, the material turns from highly flexible to rigid as the amount of polymer is increased progressively. This variation makes sense given the rigidity of the BPGE molecule used in building the bridged precursor. Besides the rigidity of the organic bridges, the evolution of the nanostructure from agglomerated nanoparticles to a continuous solid material is expected to influence the mechanical properties.

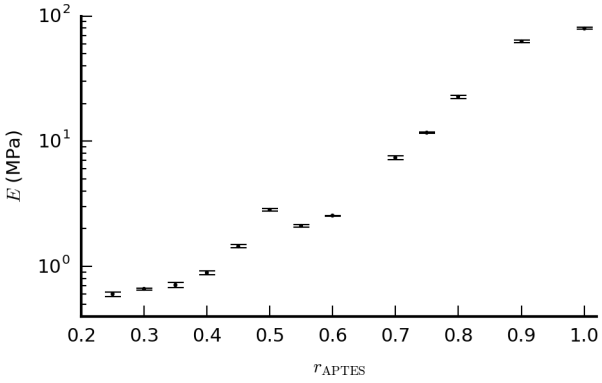

Fig. 7 Elastic modulus vs r_{APTES}. E can be tuned over two orders of magnitude by modifying r_{APTES}.

Conclusions

A monolithic, porous, low-density organic-inorganic hybrid material has been prepared via one-pot sol-gel process and subsequent supercritical drying. The material is prepared from TEOS and a bridged alkoxide previously prepared from APTES and an epoxy resin. The use of ethanol as the only solvent and the one-pot procedure minimize the environmental impact of using solvent. The material presents a micrometric pore structure that is formed by agglomerated nanoparticles or is a continuous solid depending if the proportion of bridged alkoxide in the synthesis is low or high, respectively. The mechanical properties of the material can be continuously modified by variation on this same proportion. As an example, the elastic modulus, which is in the range of polymeric foams and elastomers, changes in two orders of magnitude along the range of TEOS:bridged alkoxide proportions that generate a monolithic material. This continuous variation of the elastic modulus shows the feasibility of preparing the material with tailored mechanical properties.

Acknowledgements

MATGAS is acknowledged for allowing the use of their supercritical drying facilities. Dr Daniel Crespo (Departament de Física Aplicada, Escola d'Enginyeria de Telecomunicació i Aeronàutica de Castelldefels, Universitat Politècnica de Catalunya) is acknowledged for his help in the DMA tests. SOPREMA (France), the Spanish Ministerio de Economía y Competitividad (Grant No.

ENE-2012-36368-C02-02) and the Generalitat de Catalunya (Grant No. 2014SGR1643) are acknowledged by their financial support.

References

1. J. Livage, M. Henry and C. Sanchez, *Prog. Solid State Chem.*, 1988, **18**, 259-341.
2. A. C. Pierre and G. M. Pajonk, *Chem. Rev.*, 2002, **102**, 4243-4265.
3. R. Baetens, B. P. Jelle and A. Gustavsen, *Energy Build.*, 2011, **43**, 761-769.
4. N. Leventis, C. Sotiriou-Leventis, G. Zhang and A. M. M. Rawashdeh, *Nano Lett.*, 2002, **2**, 957-960.
5. J. P. Randall, M. A. B. Meador and S. C. Jana, *ACS Appl. Mater. Interfaces*, 2011, **3**, 613-626.
6. D. A. Loy and K. J. Shea, *Chem. Rev.*, 1995, **95**, 1431-1442.
7. K. J. Shea and D. A. Loy, *Chem. Mater.*, 2001, **13**, 3306-3319.
8. D. J. Boday, R. J. Stover, B. Muriithi and D. A. Loy, *J. Mater. Sci.*, 2011, **46**, 6371-6377.
9. M. A. B. Meador, A. S. Weber, A. Hindi, M. Naumenko, L. McCorkle, D. Quade, S. L. Vivod, G. L. Gould, S. White and K. Deshpande, *ACS Appl. Mater. Interfaces*, 2009, **1**, 894-906.
10. S. R. Davis, A. R. Brough and A. Atkinson, *J. Non-Cryst. Solids*, 2003, **315**, 197-205.
11. S. Ponyrko, L. Kobera, J. Brus and L. Matějka, *Polymer*, 2013, **54**, 6271-6282.
12. Z. Yang, A. Ni and J. Wang, *J. Appl. Polym. Sci.*, 2013, **127**, 2905-2909.
13. M. A. B. Meador, C. M. Scherzer, S. L. Vivod, D. Quade and B. N. Nguyen, *ACS Appl. Mater. Interfaces*, 2010, **2**, 2162-2168.
14. T. Noisser, G. Reichenauer and N. Hüsing, *ACS Appl. Mater. Interfaces*, 2014, **6**, 1025-1029.
15. *United States Pat.,* US 8,906,973 B2, 2014.
16. N. Hüsing, U. Schubert, R. Mezei, P. Fratzl, B. Riegel, W. Kiefer, D. Kohler and W. Mader, *Chem. Mater.*, 1999, **11**, 451-457.
17. E. J. A. Pope and J. D. Mackenzie, *J. Non-Cryst. Solids*, 1986, **87**, 185-198.
18. M. Moner-Girona, A. Roig, E. Molins and J. Llibre, *J. Sol-Gel Sci. Technol.*, 2003, **26**, 645-649.
19. K. Nakanishi, *J. Porous Mater.*, 1997, **4**, 67-112.
20. K. Nakanishi and K. Kanamori, *J. Mater. Chem.*, 2005, **15**, 3776-3786.
21. H. Schmidt, *J. Non-Cryst. Solids*, 1985, **73**, 681-691.
22. H. W. Oviatt Jr, K. J. Shea and J. H. Small, *Chem. Mater.*, 1993, **5**, 943-950.
23. M. L. Anderson, P. H. Mott and C. M. Roland, *Rubber Chem. Technol.*, 2004, **77**, 293-302.
24. J. G. Williams and C. Gamonpilas, *Int. J. Solids Struct.*, 2008, **45**, 4448-4459.
25. R. Feng and R. J. Farris, *J. Mater. Sci.*, 2002, **37**, 4793-4799.
26. M. F. Ashby, *Materials Selection in Mechanical Design (Thrid Edition)*, Elsevier Butterworth-Heinemann, 2005.
27. A. Venkateswara Rao, S. D. Bhagat, H. Hirashima and G. M. Pajonk, *J. Colloid Interface Sci.*, 2006, **300**, 279-285.